Resistance logging and NMR Saturation Mapping during Waterflooding of a Chalk Sample

A contribution to the EFP-2000 project "Displacement and deformation processes in fractured reservoir chalk"

ENS J. no. 1313/00-0008

Christian Høier & Dan Olsen

Resistance logging and NMR Saturation Mapping during Waterflooding of a Chalk Sample

A contribution to the EFP-2000 project
"Displacement and deformation
processes in fractured
reservoir chalk"

ENS J. no. 1313/00-0008

Christian Høier and Dan Olsen

Contents

Introduction

This report describes laboratory experiments conducted to test the performance of a resistance rig developed by GEUS in a collaboration with Danish Geotechnical Institute (GEO) during the EFP-2000 research project "Displacement and deformation processes in fractured reservoir chalk" (Høier, 2002). The EFP-2000 work was financed by the Danish Ministry of the Environment. The present work is financed by Dansk Olie og Naturgas A/S (DONG).

Two waterflooding experiments on a sample of reservoir chalk from the Tyra gas field are monitored in real time by a resistance method resulting in 1D resistance profiles. At two times during the experiments the waterflooding is stopped and 2D saturation maps are acquired with an NMR technique. The resistance profiles are compared with the NMR saturation maps.

Danish Research Centre of Magnetic Resonance is acknowledged for providing access to the SISCO 4.7 T experimental NMR scanner.

Flooding experiments

Materials and equipment

A cylindrical plug of Maastrichtian chalk from the oil zone of the Tyra gas field in the Danish North Sea was used in the study. Table 1 reports some petrophysical parameters of the sample, which is identified as TWC2-32. The plug was embedded in epoxy with fluid distribution plates at each plug end (Fig. 1). A total of 16 electrodes were placed in two rows, exactly on opposite sides of the sample. The electrodes were equally distributed along the length of the sample, forming 8 electrode pairs, extending 8 mm into the sample with a diameter of 1.2 mm.

All materials in the sample aggregate had low magnetic susceptibility. The first set of electrodes that was mounted on the sample was made of stainless steel. These, however, proved to be slightly magnetic, as NMR test images showed strong artifacts. The steel electrodes were then replaced by electrodes of tinned copper. These proved to be much better, though some artifacts were still present. These remaining artifacts are visible in the total intensity images (Figs. 10, 12, 14, and 16) as reduced signal intensity in regions up to approximately 2 mm from the electrodes, particularly at the electrode ends. In the fluid
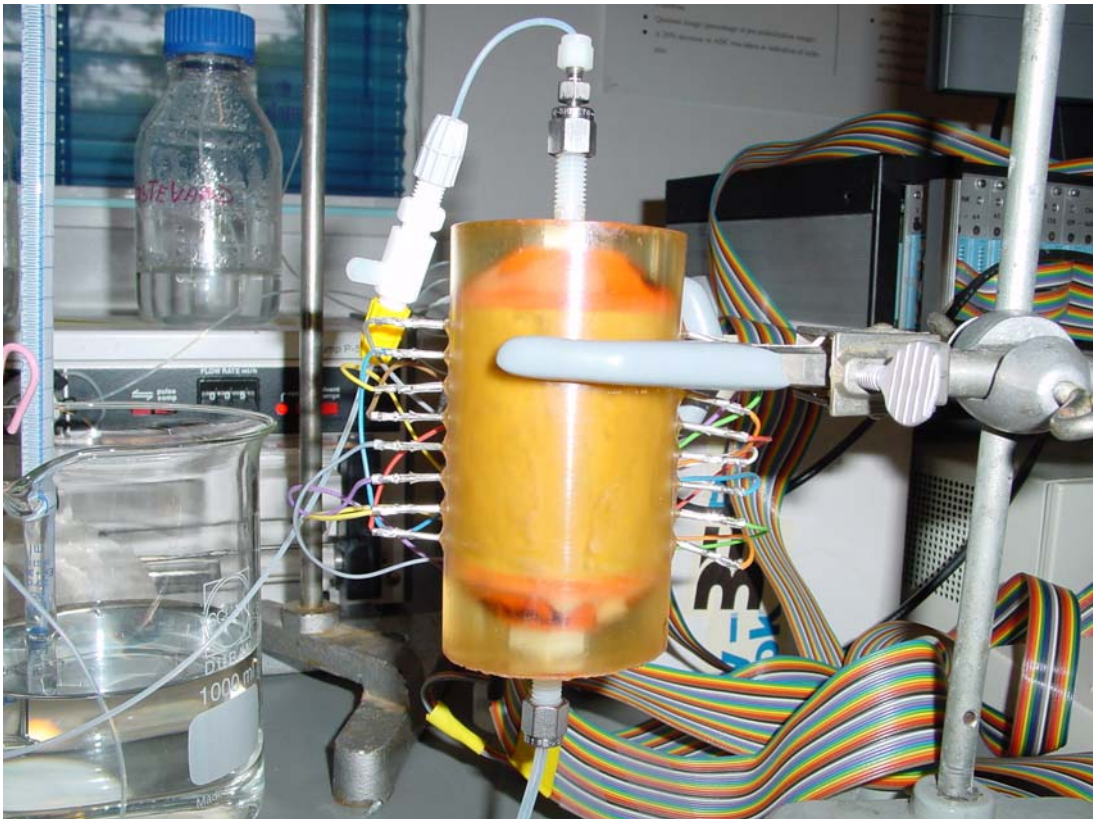
Fig. 1. Sample aggregate consisting of plug sample and fluid distribution plates (red) embedded in epoxy and 16 attached electrodes.
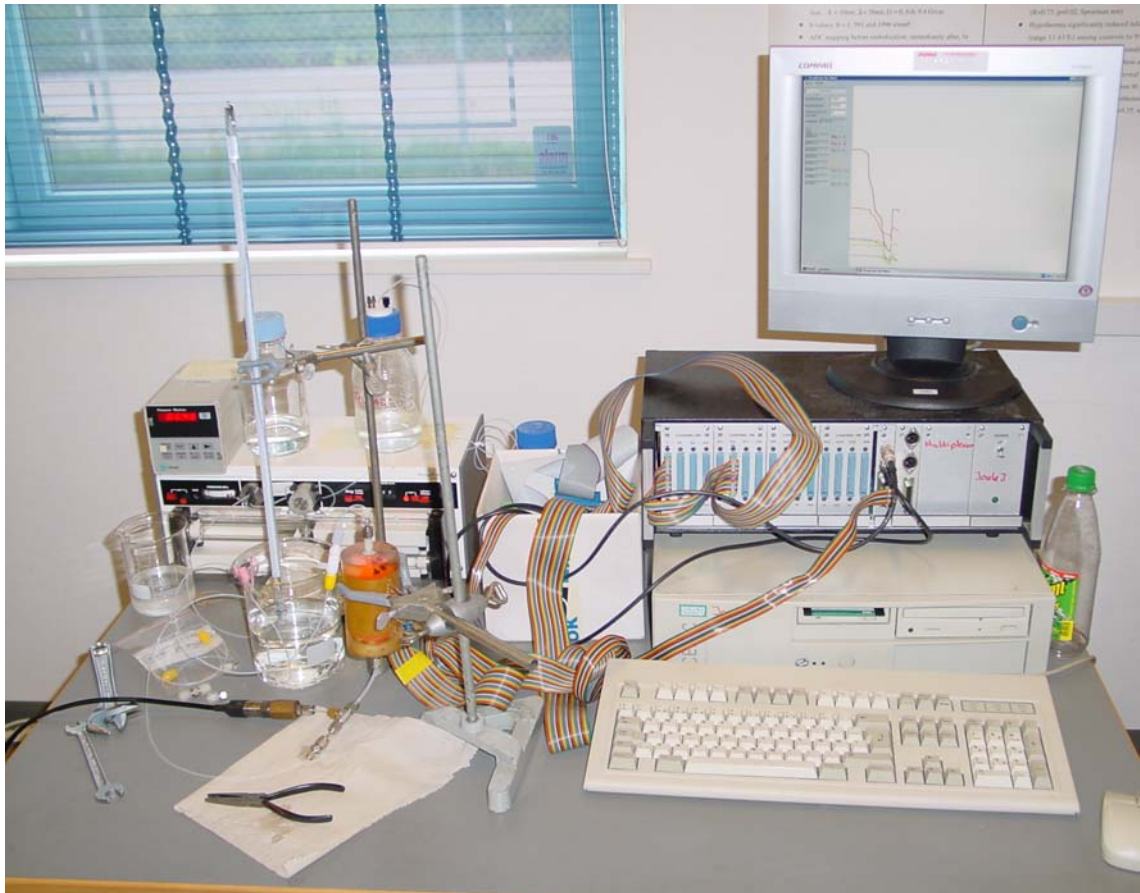
Fig 2. Experiment set-up showing, from left to right, Druck DPI 266 pressure indicator, Pharmacia P-500 pump, 25 ml burette, sample aggregate, PC, and below the computer screen the multiplexer.

saturation images (Figs. 11, 13, 15, and 17) the artifacts are much reduced. This is because the saturation images are based on intensity ratios, and the artifacts influence the oil and water signals in similar ways.

The main components of the experimental set-up are shown in Fig. 2. A fluid system consisting of Isopar-L laboratory oil (™Exxon Mobil Corp.) and tap water was used. Tap water was chosen to ascertain a good resistance level. Both fluids were degassed before use. Table 2 reports some parameters of the experimental fluid system.

Table 1. Petrophysical parameters of sample TWC2-32.	
Sample type: Cylindrical 1.5" plug sample embedded in epoxy with fluid distribution plates at each end.	
Length	= 6.45 cm
Diameter	= 3.77 cm
Bulk volume	= 71.75 ml
Porosity	= 45.91 %
Pore volume	= 32.94 ml
Liquid permeability	= 16 mD

Table 2. Fluid properties @ 22 °C.		
Fluid	Viscosity (cp)	Density (g/ml)
Water	0.95	0.998
Isopar-L oil	1.46	0.766

Sample preparation

Sample TWC2-32 had previously participated in other flooding experiments (Olsen, 1994). It contained a mixture of laboratory oil and water at the beginning of the present study. The sample had been thoroughly cleaned for heavy oil components in connection with the previous experiments. The preparation for the present experiments was a three-step flooding procedure. First, one pore volume (PV) of degassed Isopar-L oil was flooded through the sample at a rate of 10 ml/h. Then, 2.5 PV's of degassed isopropanol was flooded through the sample at a rate of 10 ml/h, and finally, 8 PV's of Isopar-L oil were flooded through the sample. Sample preparation and the following flooding experiments were all conducted at approximately 22 °C.

During cleaning the liquid permeability of sample TWC2-32 was determined to be 16 mD. This is significantly higher than the water permeability of 6 mD that was determined shortly after the sample was embedded in epoxy. The reason for the permeability increase is not known, but could possibly be related to the drilling of holes for electrodes, or wear from the participation in multiple flooding experiments.

Before the waterflooding experiment started an NMR spectrum was acquired to check for the presence of residual water. No water peak was visible indicating that any residual water was below the detection limit of $S_w = 2$ %. It is concluded that at the beginning of the flooding experiments the sample was in a state with $S_o = 100$ %.

Waterflooding experiments

Two waterflooding experiments were conducted with acquisition of resistance data and NMR data. The first experiment was a waterflood starting at S_w=0 %. A flush with oil was then conducted to reduce S_w as much as possible, and the second waterflood experiment was conducted starting from S_w=54.4 %. Table 3 gives an overview of the experiments. Each of the two waterflooding experiments comprised three flooding sessions separated by two NMR data acquisition sessions.

Waterflooding was performed with a constant rate of 5 ml/h. During the flooding sessions resistance data were collected continuously by the resistance equipment. Produced fluids

Table 3. Experiment overview. Sample TWC2-32, 26.-30. June 2003.				
Exp. step no.	Duration (hours)	Experiment no.	Task description	S_w (fraction) at end of step
1			Exp. set-up	0.000
2	0.73	Flooding exp. 1	Flooding A approximately to electrode pair 2 @ 5 ml/h	0.120
3	1.0	Flooding exp. 1	Mounting of sample in NMR scanner	0.120
4	17.0	Flooding exp. 1	NMR scanning 1	0.120
5	2.1	Flooding exp. 1	Sample handling etc.	0.120
6	2.47	Flooding exp. 1	Flooding B approximately to electrode pair 6 @ 5 ml/h	0.458
7	1.0	Flooding exp. 1	Mounting of sample in NMR scanner	0.458
8	17.0	Flooding exp. 1	NMR scanning 2	0.458
9	1.8	Flooding exp. 1	Sample handling etc.	0.458
10	2.08	Flooding exp. 1	Flooding C to S_{or} @ 5 ml/h	0.602
11	3.43		Flush to S_{wir} @ 20-50 ml/h	0.542
12	0.18	Flooding exp. 2	Flooding A @ 5 ml/h	0.585
13	1.0	Flooding exp. 2	Mounting of sample in NMR scanner	0.585
14	17.0	Flooding exp. 2	NMR scanning 3	0.585
15	1.3	Flooding exp. 2	Sample handling etc.	0.585
16	0.15	Flooding exp. 2	Flooding B approximately to electrode pair 6 @ 5 ml/h	0.607
17	1.0	Flooding exp. 2	Mounting of sample in NMR scanner	0.607
18	17.0	Flooding exp. 2	NMR scanning 4	0.607
19	4.1	Flooding exp. 2	Sample handling etc.	0.607
20	0.87	Flooding exp. 2	Flooding C to S_{or} @ 5 ml/h	0.620

were collected by a 25 ml burette that was manually read with intervals of 5 to 10 minutes. Sample inlet pressure was recorded at the same intervals. No backpressure was applied.

During waterflooding the sample was in a vertical position with the outlet end pointing upward (Fig. 1). During the oil flush sample position was reverse, with the outlet end pointing downward. During NMR measurements the sample was in a horizontal position, necessitated by the geometry of the NMR scanner (Fig. 5).

In connection with the NMR sessions flooding was stopped, and the sample was mounted in the NMR scanner. Refer to chapter "NMR measurements" for details of the NMR measurements. Handling and set-up took 0.5 to 1 hour before scanning started. The following data were collected in sequence during each NMR session:
1. A bulk spectrum. Duration of data acquisition 2 minutes.
2. The first of two water CSI images for fluid redistribution check. Duration of data acquisition 15 minutes.
3. A set of four water CSI images for quantitative fluid saturation determination. Duration of data acquisition 8 hours
4. A set of four oil CSI images for quantitative fluid saturation determination. Duration of data acquisition 8 hours.
5. The second of two water CSI images for fluid redistribution check. Duration of data acquisition 15 minutes.

Waterflood experiment 1

Waterflood experiment 1 started from a fully oil saturated condition, i.e. S_o=100%, S_w=0%. Fig. 3 presents a log of the waterflood.
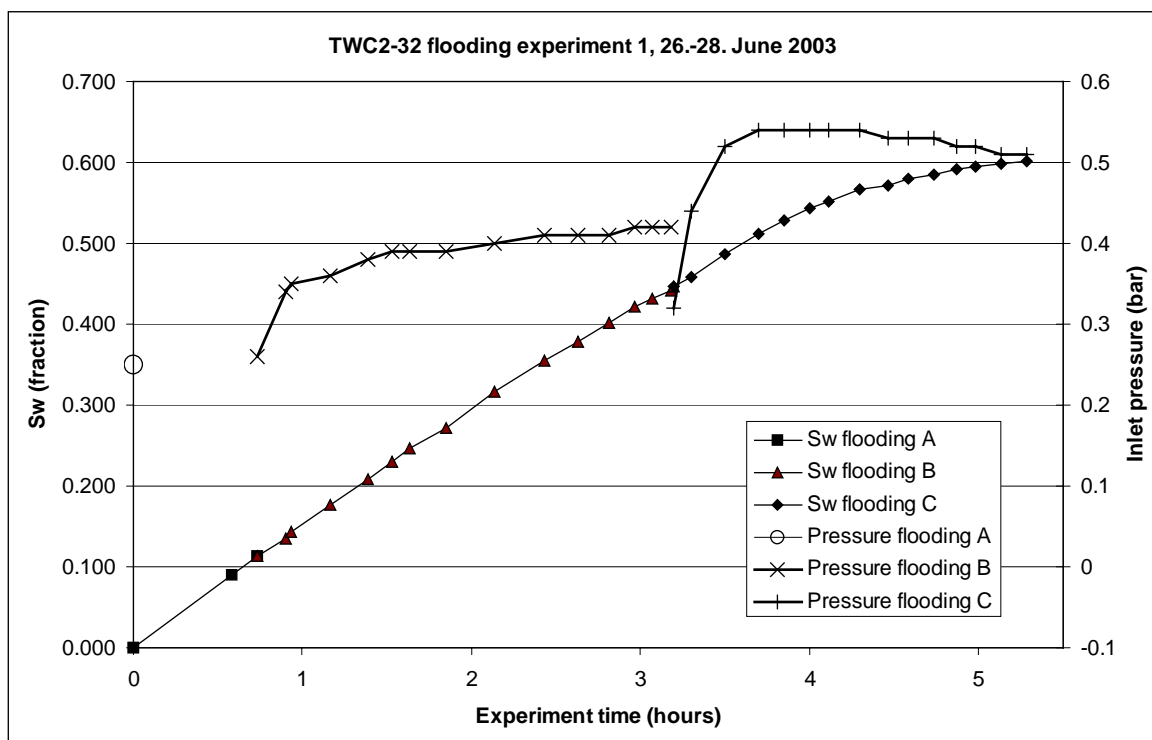
Fig. 3. Production log for Flooding experiment 1.

Water breakthrough occurred early at experiment time 1.85 h, hinting that the displacement was not piston like. After breakthrough followed a long period of two-phase production, and even at the end of the water flooding, at experiment time 5.28 h, the fractional oil flow was 0.20.

The two NMR sessions took place at experiment time 0.73 h and 3.20 h (Fig. 3). The pressure log indicates that fluid redistribution took place at these occasions.

Waterflood experiment 2

The oil flush after Waterflood experiment 1 was intended to reduce the water saturation, but unfortunately was very ineffective. It removed only pore water equivalent to 6.0 % of the sample pore volume. Waterflood experiment 2 then started from a condition with S_o=45.8 %, S_w=54.2 %. Fig. 4 presents a log of this experiment. Due to the high initial S_w very little oil was produced, only equivalent to 7.8 % of the sample pore volume.

The two NMR sessions took place at experiment time 0.18 h and 0.33 h (Fig. 4). As for the first waterflood, the pressure log indicates that fluid redistribution took place during the NMR sessions.
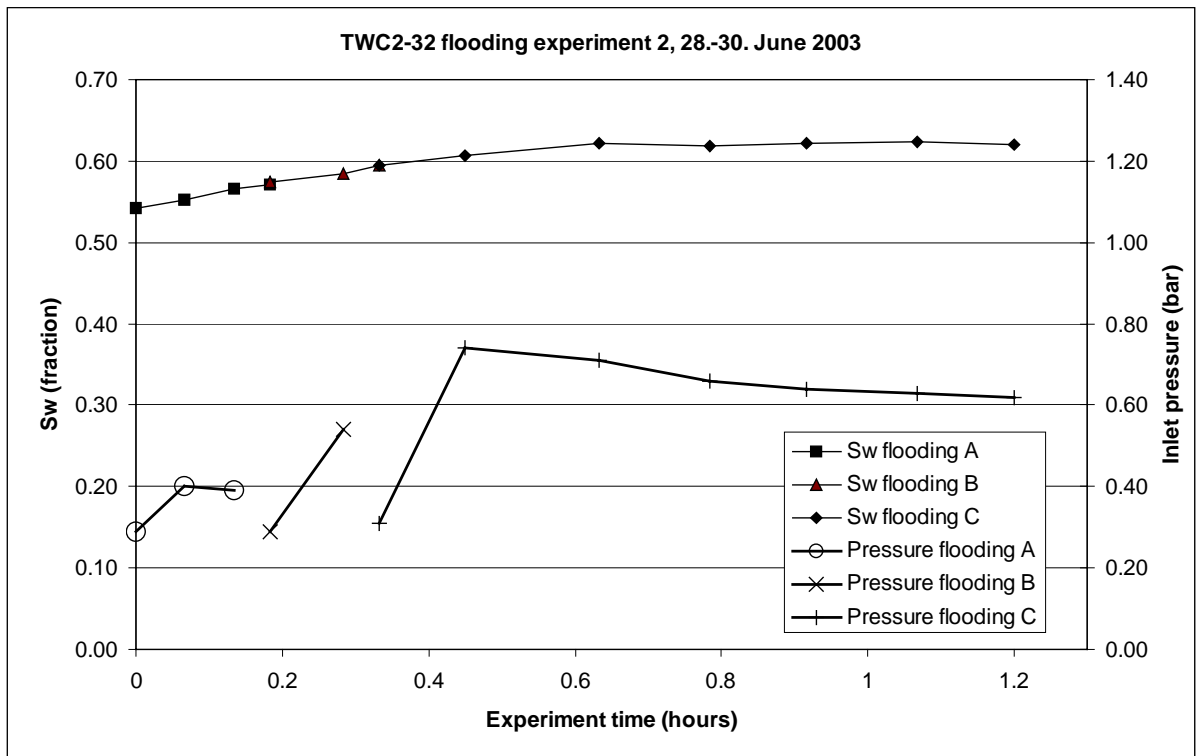
Fig. 4. *Production log for Flooding experiment 2.*

NMR measurements

NMR equipment

A 4.7 T SISCO experimental NMR scanner at Danish Research Centre of Magnetic Resonance (DRCMR) was used for the NMR work (Fig. 5). It was equipped with a 154 mm diameter insert gradient set, capable of producing magnetic gradient up to 140 mT/m along any of three orthogonal directions, with a rise rate of $5.4*10^5$ mT/m*s. The gradient set provides active shielding and eddy current compensation. A Radio Frequency (RF) coil of slotted tube resonator design with good signal homogeneity until a maximum length of 9 cm was used. The physical inner diameter of the coil is 8.5 cm, and the maximum diameter that may be used for NMR measurements is approximately 6 cm.

The equipment was tuned to detect signals from hydrogen ^{1}H at 200 MHz, and nothing else.

The scanner is controlled by SISCO's VNMR software (V.6.1) running on a Sun Sparcstation 10.

Fig. 5. The 4.7 T SISCO experimental NMR scanner at Danish Research Centre of Magnetic Resonance (DRCMR).

NMR bulk fluid saturation determination

NMR bulk saturation determinations were made with the Spectrum Integration method. In this method spectra of NMR signal intensity versus frequency are acquired from the sample. NMR signal intensity is directly proportional to the amount of hydrogen (Kleinberg & Vinegar, 1996), and if the NMR signals from the chemical compounds of the sample can be resolved in the frequency domain, integration of the signal intensities gives a measure of the amounts of the chemical compounds. In the case of sample TWC2-32 the NMR signals from water and oil in the sample were well resolved as two peaks situated approximately 800 Hz apart. Line widths measured as full width at half maximum (FWHM) were approximately 80 Hz and 150 Hz, respectively, for water and oil.

Bulk fluid saturations S_w and S_o were calculated as

$$S_w = \frac{\dfrac{M_w}{D_w}}{\dfrac{M_w}{D_w} + \dfrac{M_o}{D_o}}$$ .... (1)

and

$$S_o = \frac{\dfrac{M_o}{D_o}}{\dfrac{M_w}{D_w} + \dfrac{M_o}{D_o}}$$ .... (2)

where M_w and M_o are NMR magnetisations obtained by integration of NMR spectra, and D_w and D_o are the densities of ^{1}H in water respectively oil.

Application of Eqs. (1) and (2) forces the sum $S_w + S_o$ to be 1, i.e.

$$S_w + S_o = 1$$ .... (3)

This is justified by the careful use of degassed fluids in sample preparation.

NMR spectra are displayed in absorption mode in Figs. 6 to 9, with the resulting bulk fluid saturations given in the captions. In all four figures, the water peak is at the left and the oil peak at the right. NMR bulk saturations obtained by the Spectrum Integration method are considered accurate within 2 %-points (1 σ).
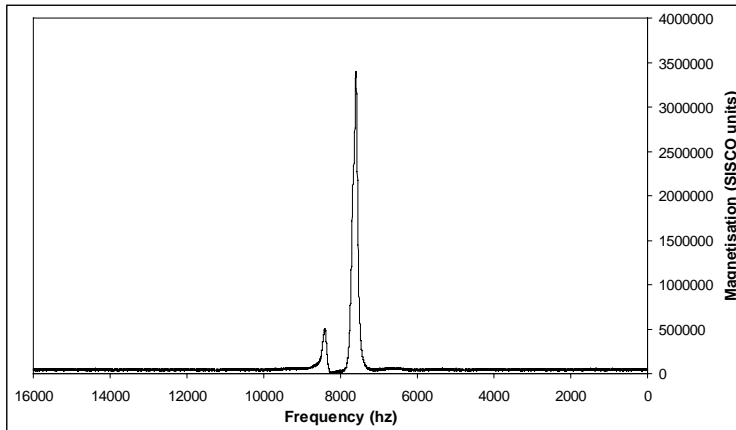
Fig. 6. NMR spectrum for flooding experiment 1, NMR session 1.
$S_w = 12.6\%$, $S_o = 87.4\%$.
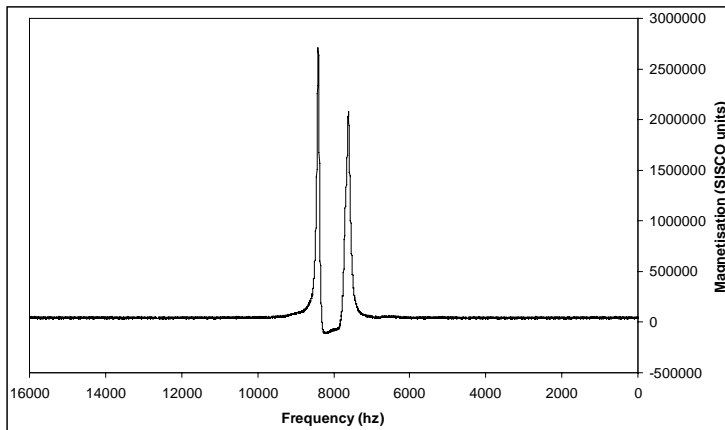
Fig. 7. NMR spectrum for flooding experiment 2, NMR session 2.
$S_w = 46.9\%$, $S_o = 53.15$.
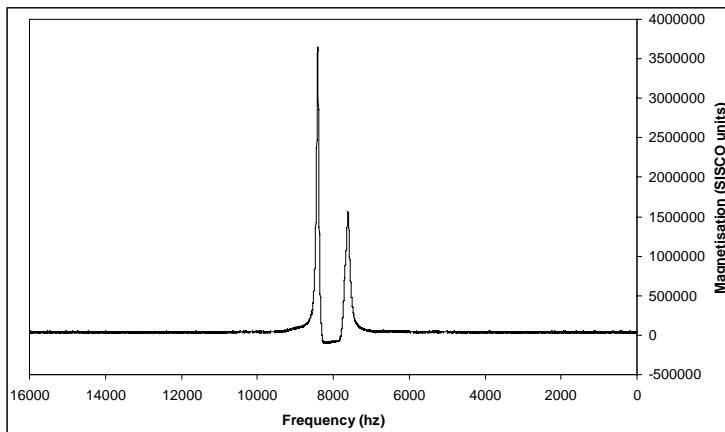
Fig. 8. NMR spectrum for flooding experiment 2, NMR session 3.
$S_w = 59.8\%$, $S_o = 40.2\%$.
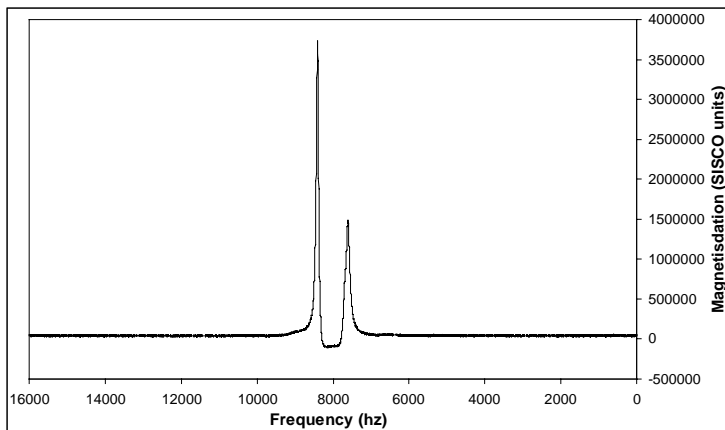
Fig. 9. NMR spectrum for flooding experiment 2, NMR session 4.
$S_w = 61.9\%$, $S_o = 38.1\%$.

NMR fluid saturation mapping

Quantitative saturation maps showing the distribution of water and oil in two spatial dimensions (2D) were produced by a chemical shift (CSI) technique which allows resolution of NMR signals at specific chemical shift values. A pulse sequence of spin-echo type used a gauss-shaped RF pulse to selectively excite the desired signal. This method requires that the water and oil resonances are well separated (Horsfield et al., 1990), which was the case for the present work, where the water and Isopar-L resonances were 800 Hz apart. Linewidths were 80 and 150 Hz respectively for the water and the oil resonance, measured as FWHM. A selective gauss-shaped pulse of duration 5.0 ms with a nominal bandwidth of 800 Hz allowed separate excitation of the two signals. Another gauss-shaped pulse was used for slice selection resulting in a slice selection profile with thickness approximately 5 mm, though somewhat irregular.

Data processing

The experimental NMR data were processed according to the following procedure to produce quantitative saturation maps in 2D.

Relaxation Correction

The effect of spin-lattice (T1) relaxation was eliminated by selecting the repetition time t_r at least 6 times the longest T1 component present in the sample. The fluid phase with longest T1 was the Isopar-L oil, and at the beginning of flooding experiment 1, where the sample was 100 % saturated with oil, T1 was measured to be 1114 ± 3 ms. A repetition time of 7000 ms was then used in all imaging experiments. This convention assured that the error on signal intensity due to differential saturation of the NMR signals was less than 0.5 % of the detected signal, even for the longest-lived component.

Spin-spin relaxation of an inhomogeneous system is a complex process, which in principle follows a multiexponential behaviour according to

$$M(t) = M(t=0) \int P(a) \exp(-t/T_2(a)) da \qquad \text{...} \quad (4)$$

where $M(t)$ is the magnetization at time t, $P(a)$ is the volume probability density function for pore size a, and $T_2(a)$ is the spin-spin time constant for pores of size a (Halperin, 1989). The spin-spin relaxation of the sample is compensated by a relaxation modelling on an array of data sets (Edelstein et al., 1988, Nørgaard et al., 1999). The array of data sets is acquired, with identical acquisition parameters, except for different values of echo time, t_e. A spin-spin relaxation model is then calculated for each pixel array, producing 2D data sets of the fitted parameters, including the magnetization at time zero, $M(t=0)$. The t_e values of the set-up are selected for optimal definition of the relaxation. Downwards the setting of t_e is restricted by system hardware constraints, which in the case of the CSI pulse sequence resulted in $t_{e,min}$, being 7.4 ms. The smallest t_e value was selected to be equal to $t_{e,min}$, in order to trace the relaxation path as close to the $M(t=0)$ condition as possible.

An important issue is the choice of spin-spin relaxation model. Bi-exponential or stretched exponential models are commonly necessary to produce reliable models (Kim et al., 1992, Kenyon et al., 1988), but a cleaned chalk sample, like the actual sample, is usually confidently modelled by a single-exponential model (Olsen et al., 2001, Bech et al., 2000, Olsen et al., 1996). Therefore, in the present work single-exponential modelling is used, i.e.

$$M(t) = M(t=0)\exp(-t/T_2) + E$$ .... (5)

where E is the signal level (noise) at $t=\infty$. In the present work 2D data sets were acquired at 4 different echo times, 7.4, 10, 16 and 30 ms, for both the water signal and the oil signal. The magnetisation of every voxel in the image plane of the sample was thus sampled at these four echo times for both the water signal and the oil signal. The single exponential model (Eq. 5) was then applied to the data from every voxel for both water and oil resulting in values for the magnetisation at time zero M(t=0) for both water and oil. The length of the model extrapolation from the minimum echo time $t_{e,min}$ to t=0 is a crucial parameter for the quality of the final saturation model: short extrapolations result in a good saturation model, long extrapolations result in a poor saturation model. A measure of the extrapolation length is the ratio $M(t=t_{e,min})/M(t=0)$. The apparent spin-spin time constant T_2^* varies from 4.5 to 12.6 ms for water and from 6.6 to 12.5 ms for oil. The low T_2^* values for water are only found in the NMR 1 and NMR 2 sessions close to the water front where S_w is low. In areas away front the water the lowest T_2^* values for water are 6.2 ms. A range in T_2^* from 6.2 to 12.5 ms implies that $M(t=t_{e,min})/M(t=0)$ varies from 0.30 to 0.55. Such extrapolations are reasonably short and are confidently modelled by the single exponential model. In the case of the low water T_2^* values close to the water front $M(t=t_{e,min})/M(t=0)$ varies down to 0.19. This results in significantly longer extrapolations causing less reliable saturation determinations, which is seen as more scatter in the saturation values close to the water front of Figs. 11 and 13.

Fluid saturation calculation
Fluid saturations were calculated for every voxel by the same procedure as for bulk fluid saturations, i.e. using Eqs. (1) and (2).

Fluid saturation maps
The results of the fluid saturation mapping are presented in Figs. 10 to 17. For each of the four NMR sessions two 2D maps are shown: A total intensity map and an oil saturation map. A water saturation map is also a result of the data processing, but since it contains exactly the same information as the oil saturation map, c.f. Eq. (3), it is not shown.

The total intensity maps, Figs. 10, 12, 14, and 16, show the total magnetisation of the image slice. It is calculated as the proton density weighted sum of the water magnetisation M_w and oil magnetisation M_o, i.e. same as the denominator of Eqs. (1) and (2). Proton density weighted magnetisation is actually a measure of porosity. The maps of this work have not been calibrated for porosity, and the inhomogeneity of the RF coil has not been compensated, so they do not qualify as porosity maps. However, in a qualitative manner it is be

lieved that most of the signal variation of the total intensity maps is due to porosity variation. Large trace fossils in the centre of the sample as well as several hairline fractures show up as structures with lower signal intensity than their surroundings. It is inferred that they also have lower porosity than their surroundings.

The oil saturation maps of Figs. 11, 13, 15, and 17 show the calculated oil distribution respectively at the time of NMR session 1, 2 , 3, and 4. The mean fluid saturation of each map is given in the caption. These fluid saturations may be compared with the fluid saturations given in Table 3. However, it must be remembered that the mean fluid saturations of Figs. 11, 13, 15, and 17 refers to a 5 mm slice through the sample, while the fluid saturations of Table 3 refers to the whole sample. The comparison shows that the bulk fluid saturations of Table 3 and slice fluid saturations of Figs. 11, 13, 15, and 17 agree within 5 percent units (p.u.).

The oil saturation map of waterflooding experiment 1, NMR session 1 (Fig. 11) shows a sharp but irregular water front in the lower half of the sample. Behind the water front the oil saturation quickly drops to approximately 40 %. The water front is distinctly irregular with a finger extending along the left row of electrodes. The area with trace fossils in the sample centre has not been entered by the water, though areas at the same level at both sides have been flooded. Ahead of the water front small areas of apparent water along the right row of electrodes are deemed to be artifacts. The apparent water situated along the top end of the sample is considered real, having flowed into the map slice along a route outside the map slice.

The oil saturation map of waterflooding experiment 1, NMR session 2 (Fig. 13) shows a nearly completed waterflood. As in NMR session 1 the water front is sharp but irregular. It has extended to the outlet, and water breakthrough took place some time ago, cf. Fig. 3 and description. Oil saturations of 100 % however remain along the upper right side of the sample, and in a connected, small area in the upper central part of the sample. Behind the water front it is noticed that the central area with trace fossils has been flooded.

The oil saturation map of waterflooding experiment 2, NMR session 3 (Fig. 15) is much different from the saturation maps of Flooding experiment 1. No water front is visible. Most of the sample has oil saturations between 30 % and 60 %, the mean oil saturation being 45 %. A minor area in upper central part of the sample has oil saturations around 68 %. This area was part of the last non-flooded part of the sample in Flooding experiment 1 NMR session 2, cf. Fig. 13. Evidently, water had difficulty entering this area, or oil had difficulty leaving the area.

The oil saturation map of waterflooding experiment 2, NMR session 4 (Fig. 17) is virtually identical to the saturation map of NMR session 3. The mean water saturation of the image slice only increased by 0.6 %-point from NMR session 3 to NMR session 4. Within the accuracy of the methods this is indistinguishable from the 2.2 %-point water saturation increase indicated by production data (Table 3).
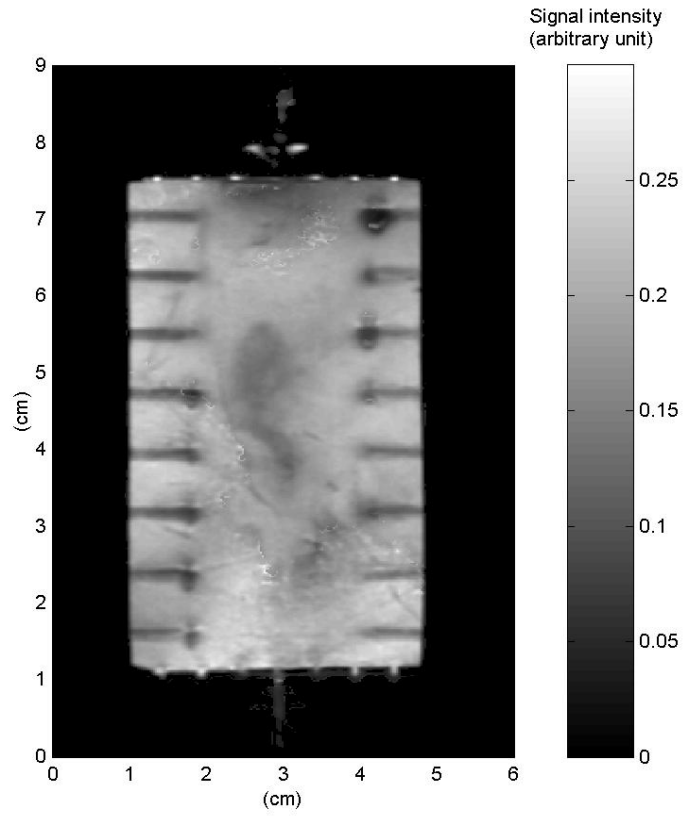
Fig. 10. Total intensity map, Waterflooding experiment 1, NMR session 1.
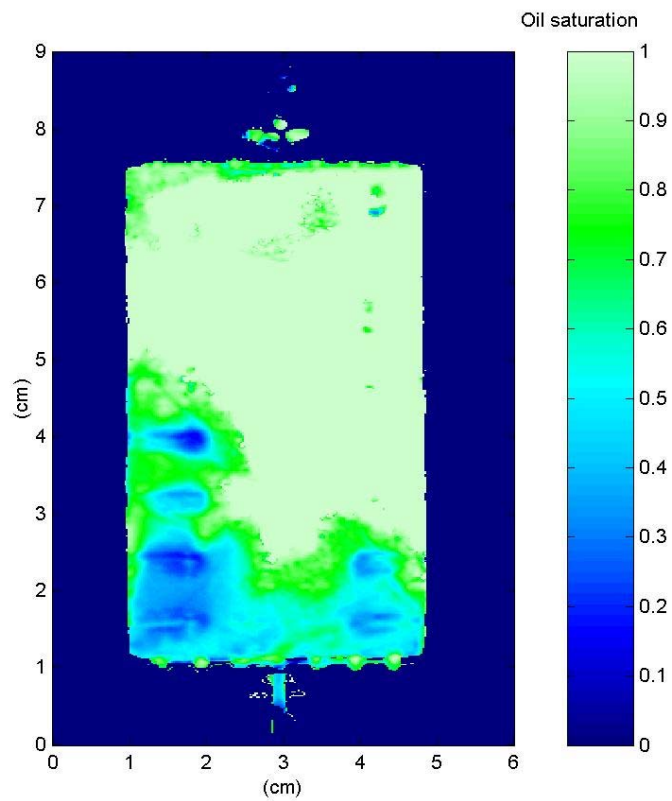
Fig. 11. Oil saturation map, Waterflooding experiment 1, NMR session 1.
Mean S_o within slice is 84.9%, mean S_w within slice is 15.1%.

GEUS   16
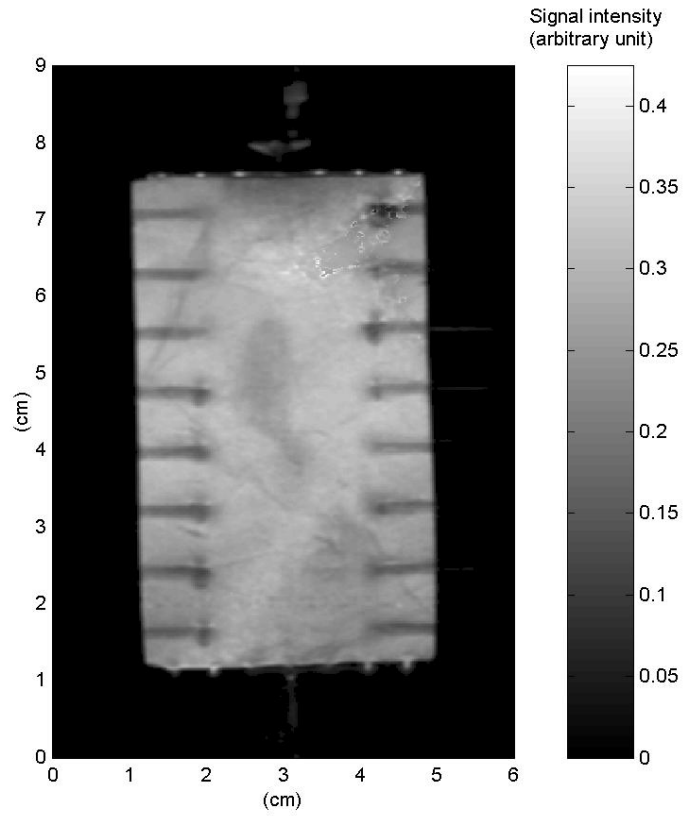
Fig. 12. Total intensity map, Waterflooding experiment 1, NMR session 2.
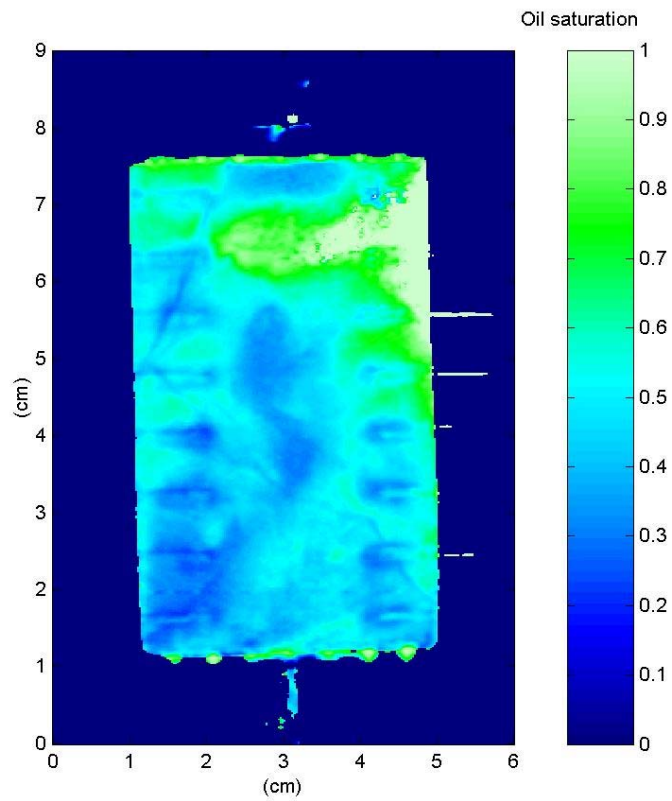
Fig. 13. Oil saturation map, Waterflooding experiment 1, NMR session 2. Mean S_o within slice is 51.7%, mean S_w within slice is 48.3%.
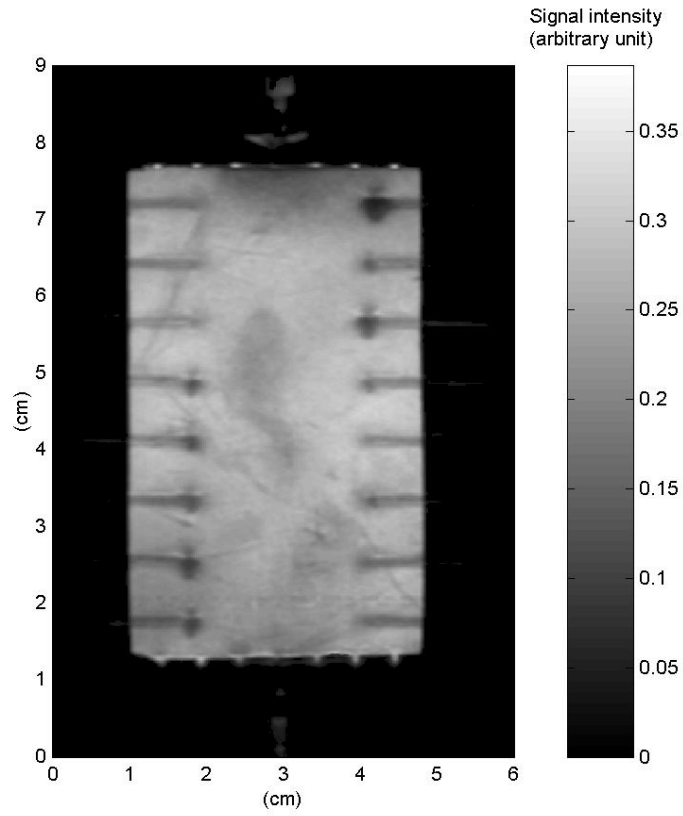
Fig. 14. Total intensity map, Waterflooding experiment 2, NMR session 3.
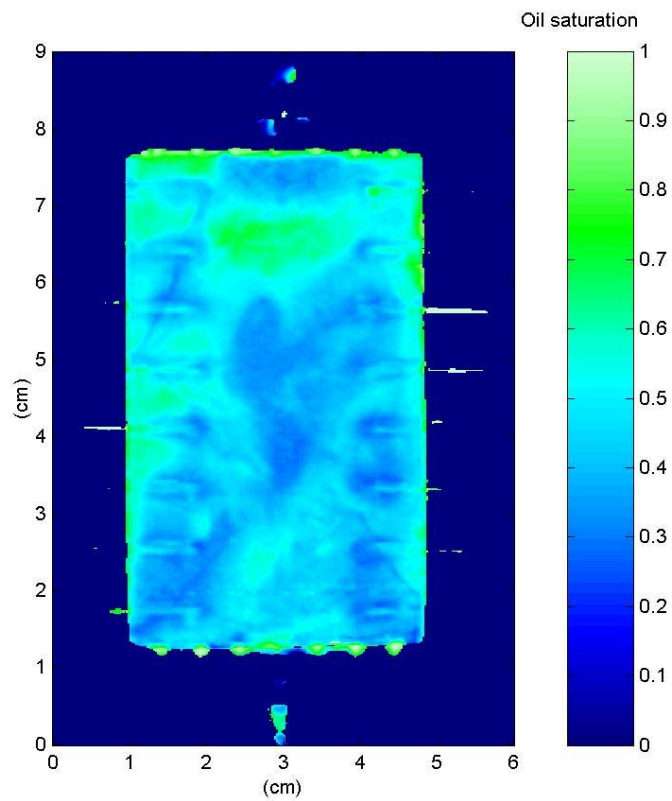
Fig. 15. Oil saturation map, Waterflooding experiment 2, NMR session 3.
Mean S_o within slice is 44.9%, mean S_w within slice is 55.1%.
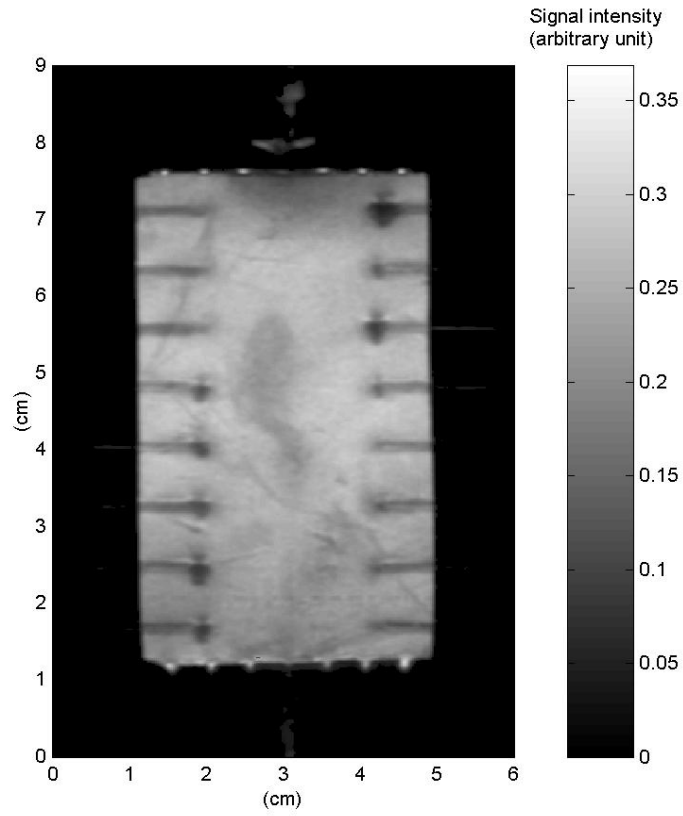
Fig. 16. Total intensity map, Waterflooding experiment 2, NMR session 4.
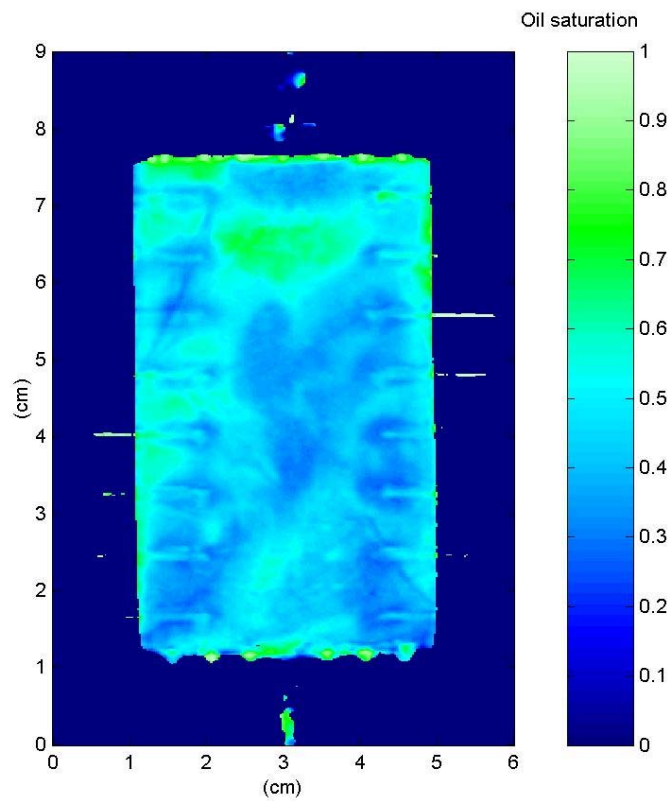
Fig. 17. Oil saturation map, Waterflooding experiment 2, NMR session 4
Mean S_o within slice is 44.3%, mean S_w within slice is 55.7%.

Fluid redistribution test

During acquisition of NMR data the flow through the sample was stopped. In this situation capillary forces are expected to redistribute the fluids within the sample to some extent. A fluid redistribution test was performed at each of the four NMR acquisition sessions to determine the extent of fluid redistribution. At the beginning of each NMR acquisition session an image of the water distribution was acquired, and a similar image was acquired at the end of each session. The difference between the two images then shows the amount of fluid redistribution. The acquisition time for these images was kept fairly low, 15 minutes for each image, to make the images as representative as possible for the state at the start and the end of the NMR acquisition session. The low acquisition time results in a poor resolution and precision for the images.

Figs. 18, 19 and 20 presents the fluid redistribution test for NMR session 1 of flooding experiment 1. All three images are presented with the same colour scale. Figs. 18 and 19 are the images for respectively the start and end of the session. Direct visual comparison reveals very little difference between the two images. Fig. 20 presents a difference image, Fig. 19 minus Fig. 18, which highlights the differences between the images. The colour scale prints values of zero as a grey colour termed "zero grey". This represents areas without change in the difference image. The major part of the difference image prints with this "zero grey" colour, indicating that no fluid redistribution took place in these areas. Shades of grey lighter than "zero grey" indicate that the water saturation of the end image, Fig. 19, is higher than the start image, Fig. 18. This is the case with a narrow zone right at the position of the water front, indicating that the water saturation **increased** during the session due to fluid redistribution. Shades of grey darker than "zero grey" indicate that the water saturation of the end image, Fig. 19, is lower than the start image, Fig. 18. This is the case with much of the area lying behind the water front where S_w was relatively high. In these areas the water saturation **decreased** during the session. The fluid redistribution test thus reveals that water flowed from the volume behind the water front to the immediate vicinity of the water front during NMR session 1. Exactly the opposite movements took place for the oil. Undoubtedly, capillary forces were responsible for the redistribution.

Fluid redistribution test. Waterflooding experiment 1, NMR session 1

Fig. 18. Water image at start of
NMR session 1.

Fig. 19. Water image at end of
NMR session 1.

Fig. 20. NMR difference image
(Fig. 19 minus Fig. 18.)

Resistance measurements

Set-up

As described in "Materials and equipment" 16 electrodes were placed on the sample. The resistance was measured across the sample from electrode 1a to 1b and electrode 2a to 2b, etc. The electrodes that are measured between are named electrode pair and the measured value is assign to a section of the sample, see Fig. 21.

Electrode: 1a   2a   3a   4a   5a   6a   7a   8a

| Section 1 | Section 2 | Section 3 | Section 4 | Section 5 | Section 6 | Section 7 | Section 8 |

Electrode: 1b   2b   3b   4b   5b   6b   7b   8b
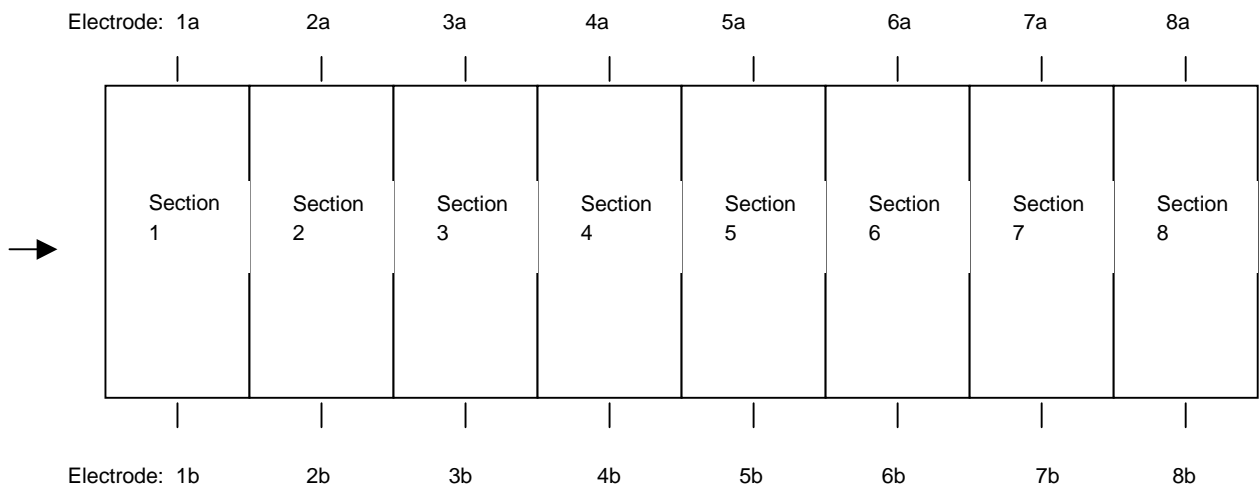
Fig. 21. Schematic cross section of the sample, showing placement of the electrode pair.

The measurements were performed by a multiplexer controlled by a PC. A generator in the multiplexer creates the voltage U_g. When an electrode pair is switched on, the multiplexer generates an electric field and the computer will measure the voltage drop U_{ref} between the electrodes over a reference resistance R_{ref}. The computer-aided multiplexer system is depicted in Fig. 22, and is visible on the photograph of Fig. 2.

The computer using the following equation calculated the resistance between a pair of electrodes.

$$R_x = R_{ref} (U_g/U_{ref} -1) \qquad\qquad (6)$$

The multiplexer system successively switches the connections between the electrodes on and off. It takes 8 measurements to get a snapshot of the resistance distribution in the chalk sample containing 16 electrodes. This was carried out by the multiplexer within 1 second. The resistance distribution was measured every 10 - 30 second during the experiments.
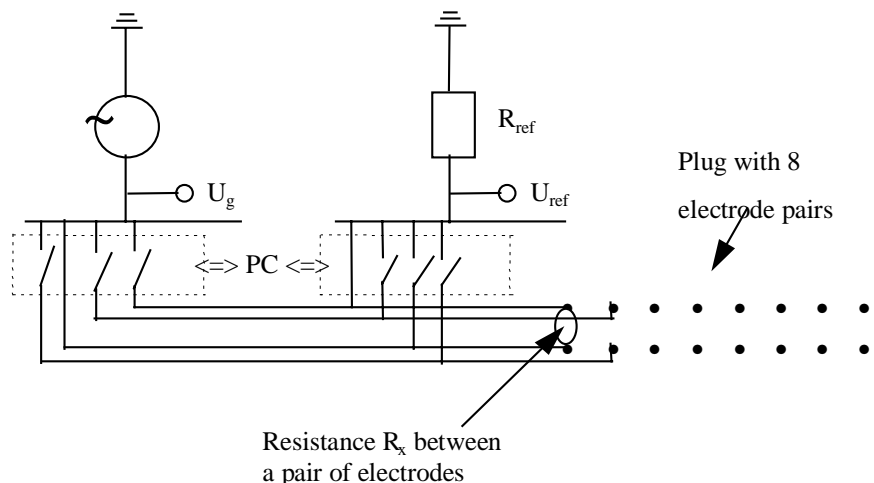
Fig. 22. Sketch of the experimental set-up showing the principle of the resistance measurements.

Resistance profile

The following resistance distribution was measured during the first experiment: waterflood of a 100 % oil saturated sample. A high resistance indicates a low water saturation in a given section and a low resistance indicates a high water saturation.

Fig. 23 shows how the waterfront is progressing in the sample as a function of time. The
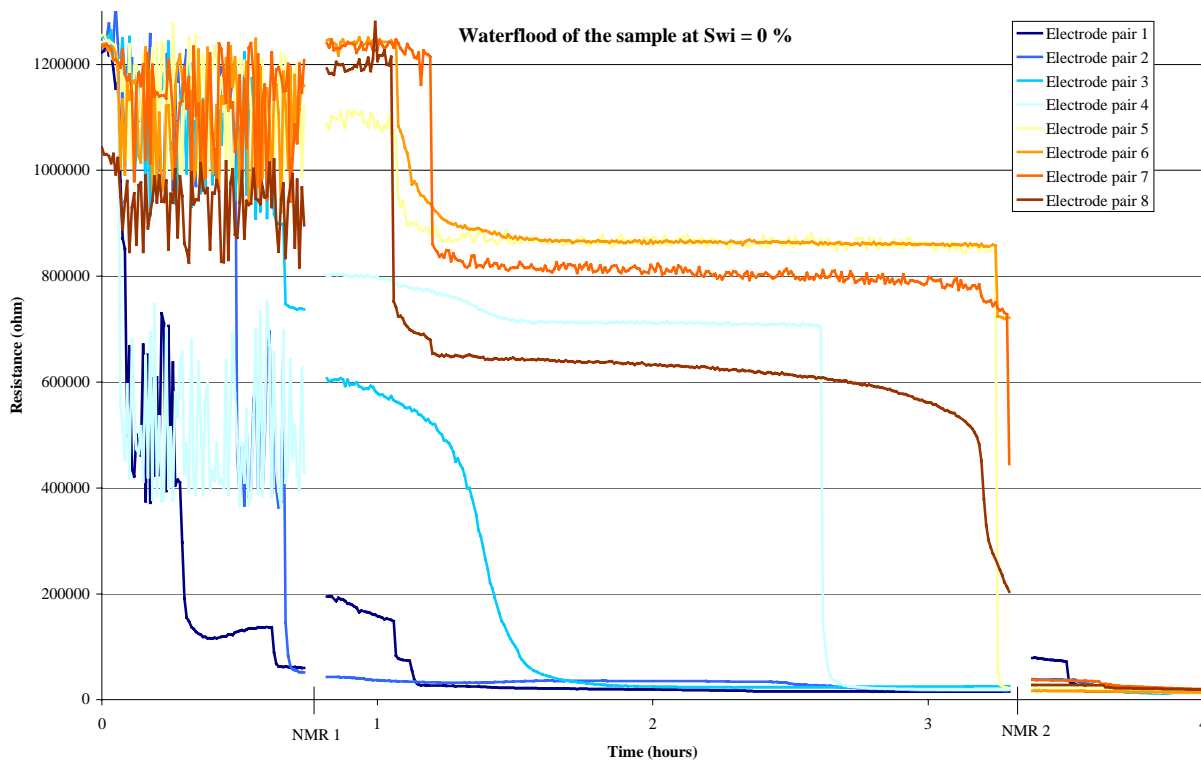
Fig. 23. Resistance profile of a waterflood in a 100% oil saturated sample.

waterfront can be seen as a drop in the resistance as water moves by the electrodes. The waterfront first meets electrode pair 1 after 0.3 hours and then electrode pair 2 after 0.7 hours, but before the resistance falls below 50.000 ohm there is a medium level at around 500.000 ohm. An oblique waterfront courses this medium level. Water has only reached the electrodes on one side of the sample, so the resistance drops to a medium level and finally down to a low level when the water have reached both of the electrodes opposite each other. This medium level can be observed for all the electrodes pair, though the medium level is a bit higher for the rest of the electrode pair, 600.000 - 900.000 ohm.

As the water rate is constant during the experiment the long offset between resistance drops of electrode pair 3 to 4, also indicates an oblique waterfront showing that water is only passing by one side of the sample.

On the x-axis are marked NMR 1 and NMR 2. This is where the experiment was stop to scan the sample using NMR. Each scanning took ~20 hours. (The scanning time has been subtracted from the figure). In that time there has been a redistribution of the water in the sample. Before NMR 1 the waterfront had passed electrode pair 1 and 2 and reached one of the electrodes in electrode pair 3. After NMR 1 the resistance of electrode pair 1 has gone up indicating water has been moved from section 1 to section 3 and 4 where the resistance had dropped to a medium level for electrode pair 3 and 4. The same observation of fluid redistribution is seen at NMR 2, where water has been moved from section 1 to section 6, 7 and 8.

At NMR 1 the resistance logs show that the waterfront has passed by electrode pair 1 and 2 and that one side of the front as reached electrode pair 3 and 4.

At NMR 2 the resistance logs show that the waterfront has reached electrode pair 8, but electrode pair 7 seems to be bypassed

The following resistance distribution was measured during the second experiment: Water-flood of a 54 % water saturated sample, see Fig. 24.

Although the waterfront was very small due to the high S_{wi} the front can still be monitored on the resistance profile, showing that the system is very sensitive. This is a contrast to the NMR saturation maps where a waterfront could not be detected. The redistribution of the water can also be seen at NMR 3 and NMR 4. The resistance of electrode pair 1 and 2 increases in both cases.

At NMR 3 the resistance logs show that the waterfront has passed by electrode pair 1 and 2.

At NMR 4 the resistance logs show that the waterfront has reached electrode pair 8
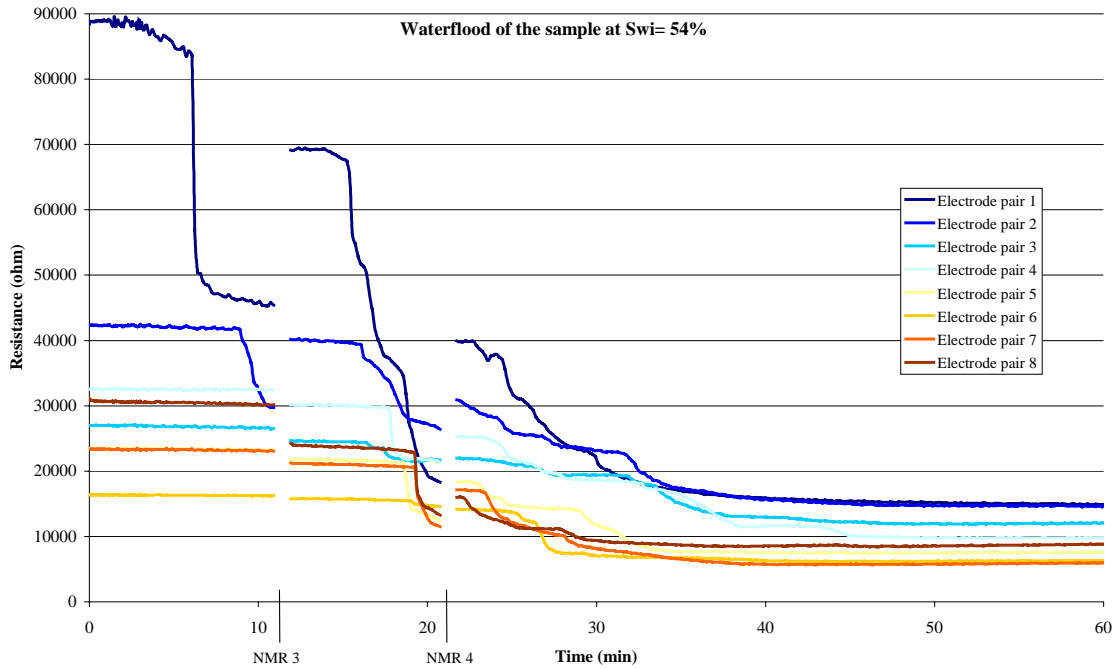
Fig. 24. Resistance profile of the sample at Swi = 54%.

Resistance profile vs. NMR images

The predicted location of the oblique waterfront in the resistance logs at NMR 1 and 2 is confirmed by the NMR saturation maps, cf. Figs. 11 and 13. It is not possible to distinguish between NMR 3 and NMR 4 because of small change in water volume using the NMR technique, but the water-front was seen by the resistance technique.

The fluid redistribution behaviour seen from the resistance logs are confirmed by the NMR difference image, Fig. 20.

The presence of a medium level in the resistance measurements indicates that a very small water-film exist on the chalk-matrix as chalk itself is not conductive. And that at initial stage the total water volume must be less than 2% of the pore-volume, which is the detection limit of the NMR technique. This is possible solution considering the used cleaning technique.

Conversion of resistance to saturation

The measured resistance is regarded as a function of the volume of water between elec-trodes and can therefore be translated to a water saturation.

Mathematical solution

To determine a correlation between water saturation and resistance an implicit method was developed by Olsen (1990). This method assumes that each electrode is measuring the true water saturation.

The aim is to find a function $S_w = S_w(R)$, which minimises the volume balance error δ_j . The volume balance error δ_j is defined as the difference between the actual water volume in the sample and the water volume measured by the electrodes.

$$\delta_j = V_{wj} - \int S_w \, \phi \, dV \quad \approx V_{wj} - \sum_{l=1}^{E} S_{wjl} \, \phi_l \, V_l \quad \text{...} \quad (7)$$

Where:

V_{wj}	=	the actual water volume in the fracture model
E	=	the number of electrodes
S_{wjl}	=	the measured water saturation at the l'th electrode in the j'th calibration point.
ϕ_l	=	the porosity of the l'th part of the volume
V_l	=	the bulk volume of the l'th part of the volume

The function $S_w = S_w(R)$ has the following form:

$$S_w = \frac{C_1}{R^4} + \frac{C_2}{R^3} + \frac{C_3}{R^2} + \frac{C_4}{R} + C_5 \quad \text{...} \quad (8)$$

A function G is introduced with the aim of finding the curve with the best fit through the measured resistances.

$$G(c_1, c_2, c_3, \ldots c_m) = \sum_{j=1}^{n} \delta_j^2 \quad \text{..} \quad (9)$$

where n is number of calibration points.

To minimise $G(c_1, c_2, c_3, \ldots c_m)$:

$$\frac{\partial}{\partial c_i} G(c_1, c_2, c_3 \ldots c_m) \quad = \quad \frac{\partial G}{\partial c_i} \quad = \quad 2 \sum_{j=1}^{n} \frac{\partial \delta_j}{\partial c_i} \delta_j \quad = \quad 0 \quad \text{...................} \quad (10)$$

The value of constants $(c_1, c_2, c_3, \ldots c_m)$ which minimise the volume balance error δ_j can now be found by inserting δ_j and $\partial \delta_j / \partial c_i$ into Eq. (10).

Conversion curve

The resistances profile was measured in successive time steps, as water was injected into the sample. Calibration data was obtained at water saturations from 0 % to 60 % in experiment 1 and from 54 % to 62 % in experiment 2. The best calculated fit lead to the following Fig. 25.
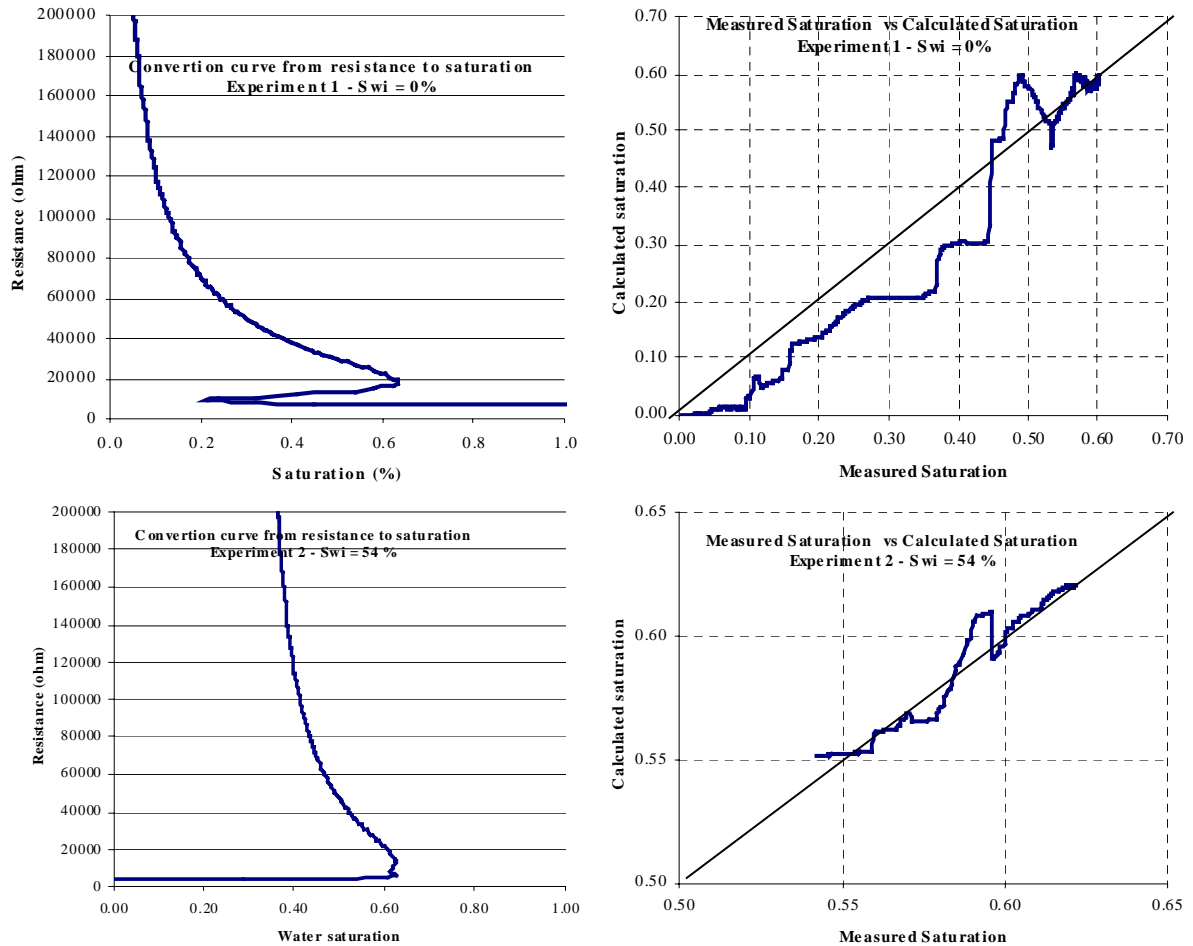
Fig. 25. Left: Water saturation as a function of resistance. Right: Water saturation measured by the electrodes and plotted against the actual water volume injected into the sample.

In both experiments there are not a very good agreement between the measured water volume and the actual injected water volume. The conversion curves are ambiguous below 20.000 and 12.000 ohm. These errors are introduced because the following assumptions are **not** valid in the experiments:

- Stable and piston like waterfront.
  Water is bypassing the electrodes on one side of the sample in experiment 1 and thereby the electrodes "see" less water than the actual volume. This is also seen from Fig. 25. In experiment 2 the waterfront is very small, due to the high S_{wi} at the start of the experiment.

- Unique boundaries around the electrodes.
  The redistribution of water at each NMR scan turns each experiment into 3 individual experiments, (Before, between and after the NMR scans) with each unique boundaries around the electrodes. Combining these data is what really troubles the calculations.

- A homogeneous sample.
  An inhomogeneous sample will lead to errors in the calculation as the total pore volume dived equal among the 8 sections.

On the following Figs. 26 and 27 the resistance profile has been converted to a saturation profile and in addition 2 lines have been added. The "Average electrode" shows the converted average saturation in the sample and the "Average saturation" is determined from the water injection and is the "true" saturation of the sample.
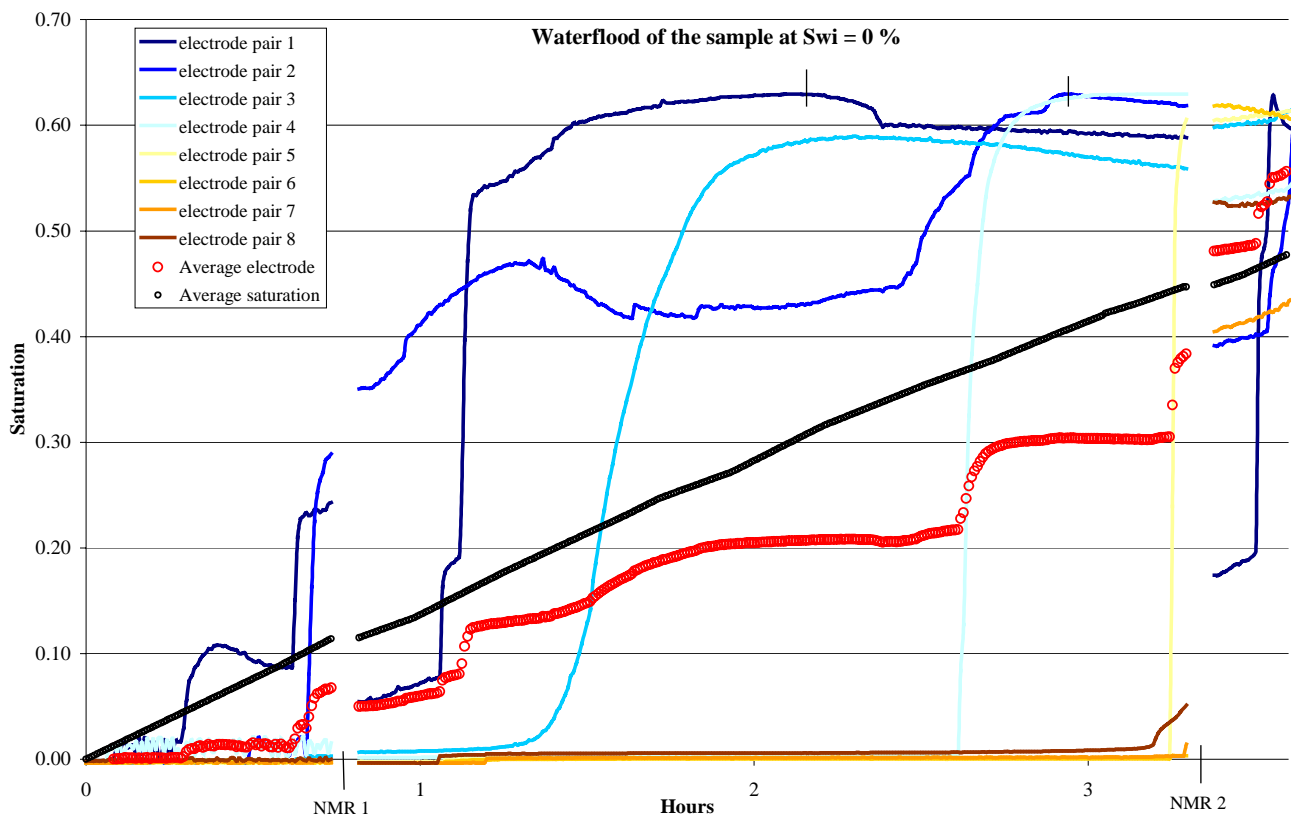
Fig. 26. Saturation profile for experiment 1.

The waterfront can be seen in both Figures as an increase in water saturation as the water passes by the electrode pairs. Comparing the "Average electrode" and the "Average saturation" in Fig. 26 shows that the converted saturation is a bit underestimated. The jump in "Average electrode" saturation between NMR scans shows that the redistribution of water affects the results. Given the circumstances the saturation conversion is rather robust and gives a decent result.
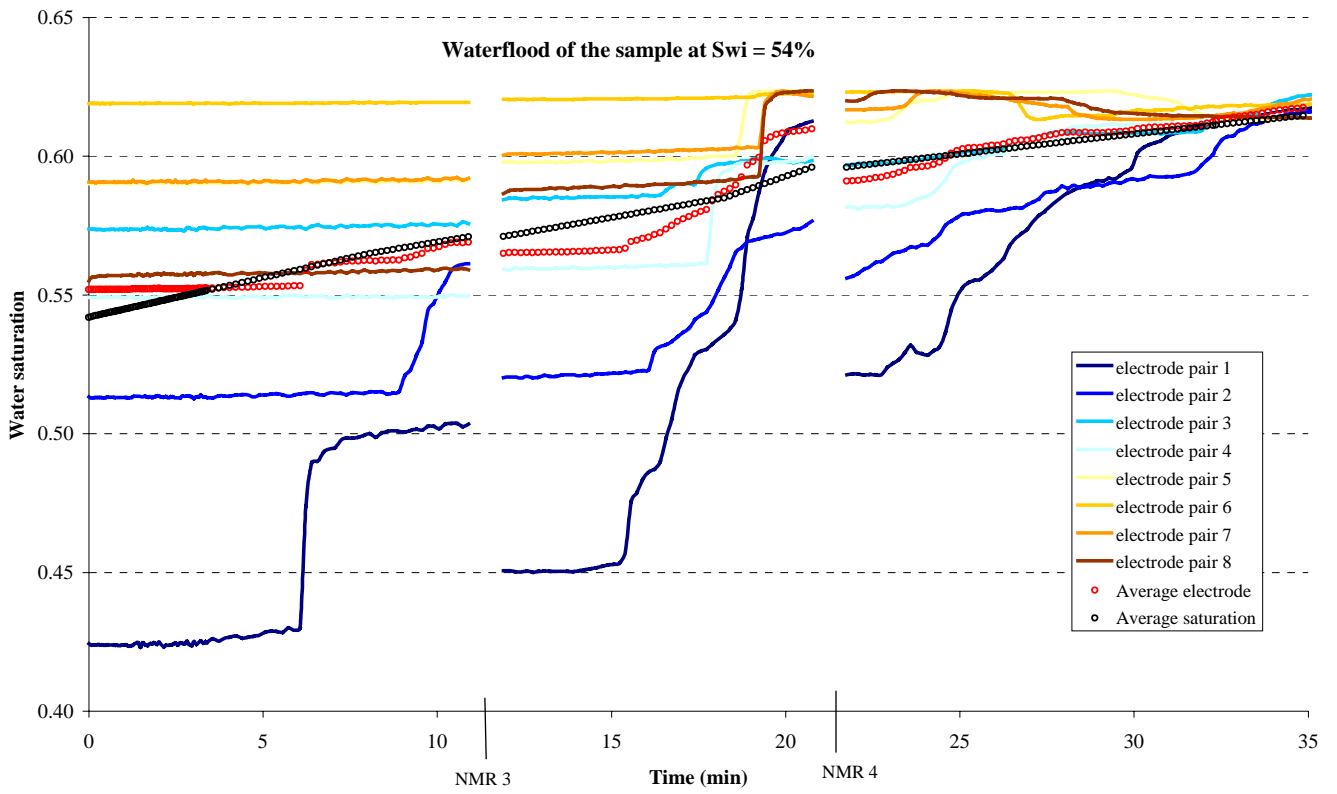
Fig. 27. Saturation profile for experiment 2.

Summary and conclusions

Two waterflooding experiments were conducted on a sample of North Sea reservoir chalk in order to test the ability of a newly developed resistance rig to produce 1D saturation profiles. During flooding resistance data were continuously recorded by the resistance equipment. In each flooding experiment two periods with interrupted flow were placed, during which 2D NMR saturation data were collected.

One experiment started from a fully oil saturated state (S_o = 100 %), the other started from an intermediate saturation state (S_o = 46 %).

Two circumstances caused the experiments to be less than ideal for the purpose of testing the performance of the resistance rig:

* The NMR saturation measurements had to be conducted in periods without flow. This caused the fluids to redistribute due to capillary forces, and usually simple relationship between resistance and fluid saturation became much more complicated.
* The selected chalk sample TWC2-32 proved to be slightly fractured and quite inhomogeneous, which caused the flooding processes to deviate much from a piston-like displacement process. This invalidated the underlying assumption of a homogeneous porous medium, making the fluid saturation calculation more uncertain.

In spite of the difficulties the following conclusions may be drawn:

1. The functionality of the resistance equipment was demonstrated, in particular the collection of 8 simultaneous resistance logs with a time resolution down to 1 second.
2. The resistance equipment generated data sets that were both internally consistent and consistent with the NMR saturation data. It was demonstrated that the resistance logs were able to predict the location of a waterfront and that the occurrence of an intermediate resistance level was caused by the waterflooding of only one of the electrodes in an electrode pair by an oblique water front.
3. Comparison with the NMR fluid redistribution check data demonstrated that the measured resistance was highly sensitive to small changes in fluid saturation. This makes the resistance method very useful for studying subtle changes in fluid saturation during experimental work.
4. The capability of the NMR CSI method to produce 2D fluid saturation maps with an accuracy of 2 %-point was confirmed.

References

Bech, N., Olsen, D. & Nielsen, C.M. 2000: Determination of Oil-Water Saturation Functions of Chalk Core Plugs from Two-Phase Flow Experiments. Reservoir Evaluation and Engineering **3,1**, 50.

Edelstein, W.A., Vinegar, H.J., Tutunjian, P.N., Roemer, P.B. & Mueller, O.M. 1988: NMR imaging for core analysis. Society of Petroleum Engineers paper **18272**, 101.

Halperin, W.P., D'Orazio, F., Bhattacharja, S. & Tarczon J.C. 1989: Magnetic resonance relaxation analysis of porous media. In: Klafter, J. & Drake, J.M. (eds.): Molecular dynamics in restricted geometries. John Wiley & Sons, New York, 311.

Horsfield, M.A., Hall, C. & Hall, L.D. 1990: Two-Species Chemical-Shift Imaging Using Prior Knowledge and Estimation Theory. Application to Rock Cores. J. Magnetic Resonance **87**, 319.

Høier, C. 2002: EFP-2000: Displacement and deformation processes in fractured reservoir chalk. Danmarks og Grønlands Geologiske Undersøgelse Rapport 2002/79, 19 pp + appendices.

Høier, C., Rosendal, A. & Lindgaard, H. F. 1999: Experimental and numerical analysis of water-oil displacement in fractured porous media. GEUS report 1999/66, Geological survey of Denmark and Greenland.

Kenyon, W.E., Day, P.I., Straley, C. & Willemsen, J.F. 1988: A three-part study of NMR longitudinal relaxation properties of water-saturated sandstones. SPE Formation Eval. **3,3**, 622.

Kim, K., Chen, S., Qin, F. & Watson, A.T. 1992: Use of NMR imaging for determining fluid saturation distributions during multiphase displacement in porous media. Society of Core Analysts paper **9219**, 18 pp.

Kleinberg, R.L. & Vinegar, H.J. 1996: NMR properties of reservoir fluids. Log Analyst **37,6**, 20.

Lindgaard, H. F. & Høier, C. 1998: Experimental and numerical analysis of two-phase flow in fractured porous media. GEUS report 1998/33, Geological survey of Denmark and Greenland.

Nørgaard, J.V., Olsen, D., Reffstrup, J. & Springer, N. 1999: Capillary-pressure curves for low-permeability chalk obtained by nuclear magnetic resonance imaging of core-saturation profiles. SPE Reservoir Eval. & Eng. **2,2**, 141.

Olsen, D. 2001: Application of non-destructive imaging methods to core analysis. In: Fabricius, I. (ed.): Nordic Petroleum Technology **V**, 89.

Olsen, D., Topp., S., Stensgaard, A., Nørgaard, J.V. & Reffstrup, J. 1996: Quantitative 1D saturation profiles on chalk by NMR. Magnetic Resonance Imaging **14,7/8**, 847.

Olsen, D. 1994: MRI of a waterflood on a reservoir chalk sample. Magnetic Resonance Imaging **12,2**, 215.

Olsen, N.K. 1990: Two-Phase Flow in Fractured Porous Media. Laboratory for Energetics, Technical University of Denmark.